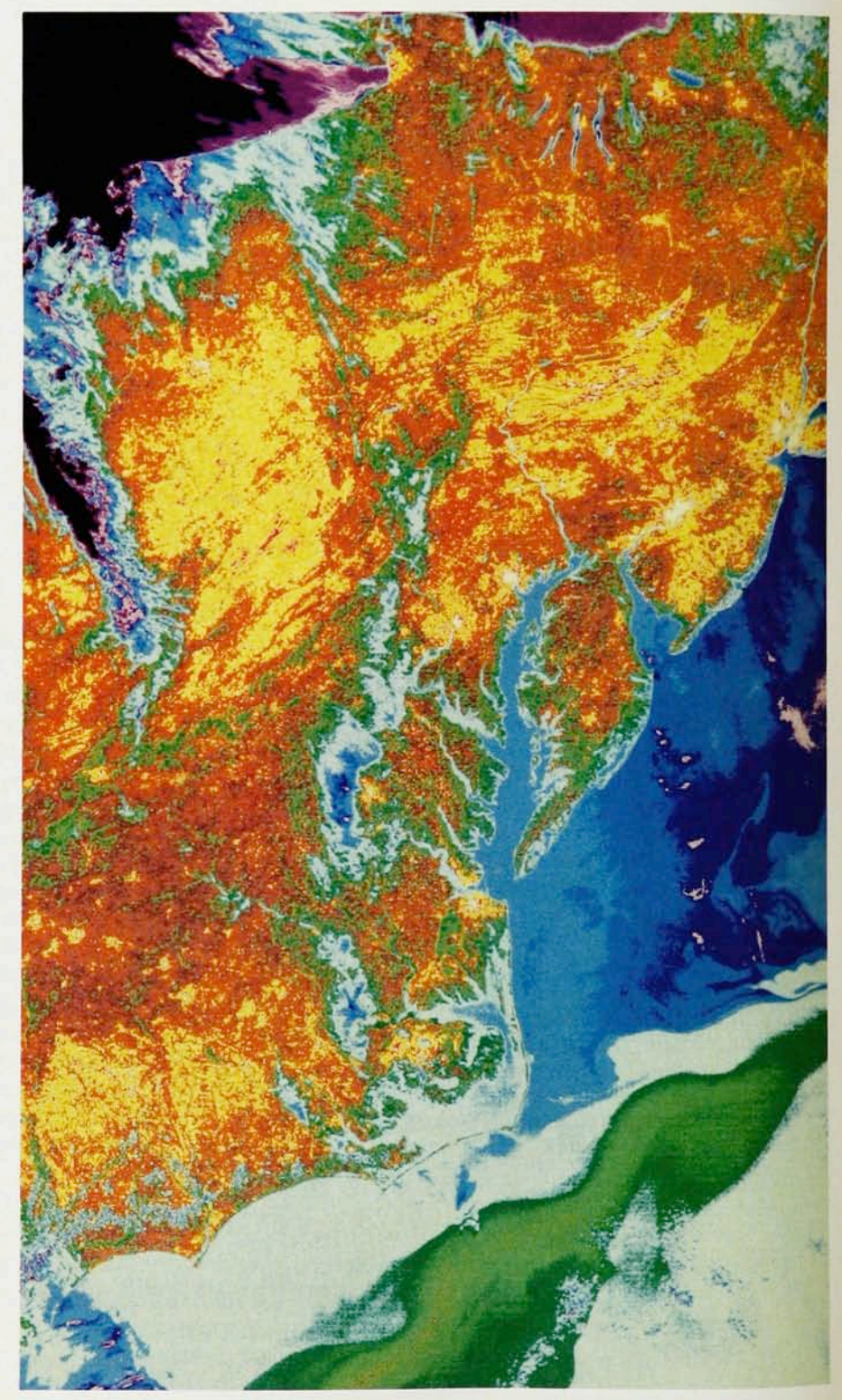
# REMOTE SENSING OF THE EARTH: A SYNOPTIC VIEW



Thermal image of the East Coast in the daytime, from the southern tip of Long Island to South Carolina, illustrating "urban heat islands." This image was taken by the Heat Capacity Mapping Mission. In it, urban areas, such as New York, Philadelphia, Baltimore and Washington, DC, appear white (hot), while the surrounding areas appear brown or green (cooler). The black and purple shapes at the upper left are clouds. At the lower right, the warm Gulf Stream water appears as a green streak in the cooler waters that surround it. The full spectrum of colors, from coldest to hottest, is: black, purple, blue, light blue, green, orange, yellow, white. (Photo courtesy of Locke Stuart, NASA-Goddard Space Flight Center). Figure 1

Space-based and aerial images can provide information about Earth resources, agricultural conditions, weather patterns and a host of other phenomena that would be impossible to observe from the ground.

John R. Schott

Remote sensing of the Earth may be traced back to the first prehistoric explorer who climbed a nearby hill to study the lay of the land. But it was not until 150 years ago that Louis Jacques Mande Daguerre and Joseph Nicéphore Niepce invented the daguerreotype, which provided the foundation for modern photography and, through it, a means to record a remotely sensed image. Twenty years later, in 1859, Gaspard Félix Tournachon Clateu (later known in the literature as Félix Nadar) took the first known aerial image from a balloon.1 That set the stage for the use of balloon-based cameras by Union troops to photograph Confederate defenses around Richmond, Virginia, during the Civil War. Kites were also used as platforms for early photography.2 A particularly notable example is a very-large-format image (1.4×2.4 m) taken by G. R. Lawrence after the 1906 San Francisco earthquake and fire. A cluster of 17 kites flown from a ship in the bay carried the camera aloft. The first known photos from an aircraft were taken in 1909 in Italy by a passenger in a plane piloted by Wilbur Wright. Aerial photography was used for reconnaissance during World War I and was further developed for that purpose during World War II, resulting in the creation of special cameras and films, including color and color infrared film for detecting camouflage.

The first rocket-based images of Earth were acquired in the early postwar period by cameras carried on a V-2 rocket, and the first images of Earth from space were acquired only 30 years ago, by the Explorer-6 satellite. Shortly thereafter, in 1960, NASA launched the first systematic space-based observation platform, the tiron-1 meteorological satellite. In that same year the world learned of the existence of high-flying reconnaissance aircraft when a U-2 piloted by Francis Gary Powers was shot down over the Soviet Union. The synoptic perspective gained with these high-altitude and space-based systems motivated the development of the satellite imag-

ing systems available today.

The various imaging requirements for different applications led to development efforts along several paths during the 1960s and 1970s. For example, the manned space program spawned several programs for collecting photographs from low near-equatorial orbits, and NASA and the National Oceanic and Atmospheric Administration placed numerous meteorological satellites in polar orbit. These meteorological systems sent down images either in real time or stored until in sight of ground stations. Limitations in on-board storage capacity and downlink bandwidth restricted the capacity of these systems to small numbers of images with relatively low resolution. Later, meteorological satellites were launched into equatorial orbits at an altitude of 22 000 miles. At this height, the angular velocity of the satellite matches that of the Earth, and thus the satellite remains stationary relative to the ground (and to the receiving station). To exploit their ability to continuously view a region, the satellites were equipped with both visible and infrared cameras for 24-hour use—a particularly valuable feature for meteorological studies. (See figure 1.)

In 1972 NASA launched the first Earth Resources Technology Satellite (later renamed Landsat I) into a lowaltitude polar orbit. With its repeat coverage cycle of 18 days and high-resolution sensors, Landsat was the first platform capable of making detailed studies of geographic phenomena. The fine resolution of the imaging sensors increased the quantity of information per image to the point that very few images could be stored on board. To avoid loss of data, NASA constructed and operated receiving stations around the globe, at considerable expense. In the mid-1980s NASA initiated the Tracking and Data Relay Satellite System as a more economical means of getting the most information from its imaging satellites. NASA positioned three geostationary (that is, equatorial geosynchronous) TDRSS satellites such that at any time at least one of them was in the line of sight of any imaging satellite, while at least one was in the line of sight of a single ground station. Thus any satellite signal could be relayed through one or more TDRSS satellites to a central ground facility.

### Observable physical parameters

To provide a framework for discussing sensors and applications, I will briefly review the observable physical parameters and the radiation physics that relates to remote sensing. To keep the problem manageable, I will consider only passive imaging systems, which operate in the energy region encompassing the visible through thermal infrared bands (0.4–20  $\mu$ m). (The vast array of sensors, analysis techniques and areas of application of remote sensing are well covered in reference 3.)

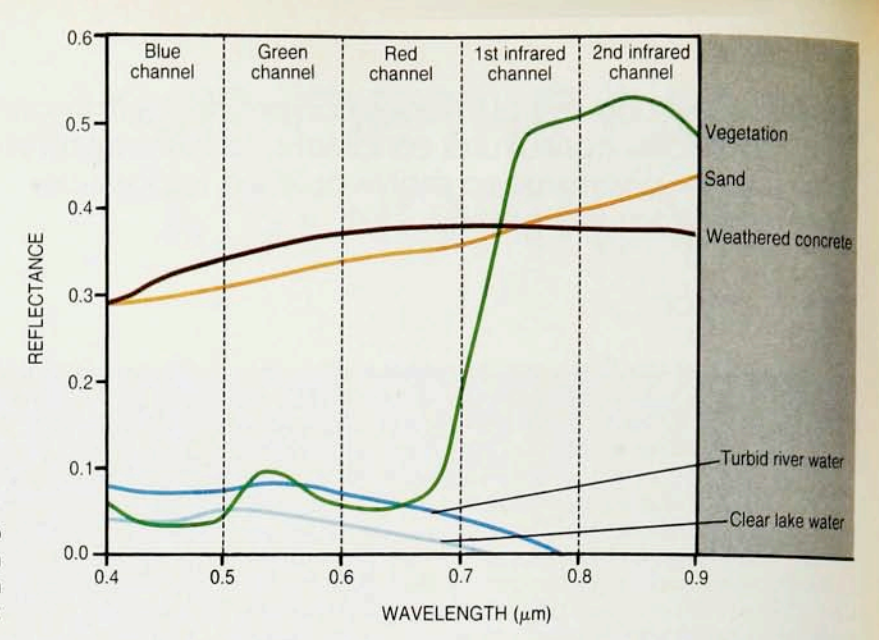
Remote sensing relies on the premise that the information of interest has a radiometric manifestation, or "signature." The simplest example of a physical signature is the variation in reflectance over a broad spectral range. This was recorded, for example, on the black-and-white aerial photos used for reconnaissance during World War II. Reflectance as a function of wavelength, which is studied with multispectral sensors, is a more complex example. Spectral reflectances vary with the land cover class or with different characteristics within a class (see figure 2).

Another type of information with a radiometric manifestation, particularly in the long-wave infrared region, is surface temperature. By carefully accounting for emissivity and atmospheric effects, one can compute surface temperature from the radiance recorded by long-wave infrared imagers.

The radiometric manifestations of the material properties one wishes to observe must, of course, exceed the radiometric resolution of the sensor. For example, significant changes in chlorophyll concentration in a body of

**John R. Schott** is a professor of imaging science and head of the Digital Imaging and Remote Sensing Laboratory at the Rochester Institute of Technology in Rochester, New York.

73



Radiometric signatures can be used to discriminate land cover types, as shown by these spectra of some common ground covers. Figure 2

water result in reflectance changes of only a few tenths of a percent, so resolutions of that magnitude would be required to observe the phenomenon.

Another kind of resolution of an imaging system—the spatial resolution—defines the size of the objects that can be observed. This is most commonly expressed in terms of the size of the detector element (a pixel, in a digital image) projected onto the ground, which represents the smallest area sampled by the system. It is referred to as the ground instantaneous field of view.

## Radiation physics

Of the many conceivable paths of travel for the radiation reaching an airborne or satellite imaging system, four are by far the most important. Shown schematically in figure 3, each of these four paths contributes one term to the standard approximate equation for spectral radiance used by remote-sensing scientists:

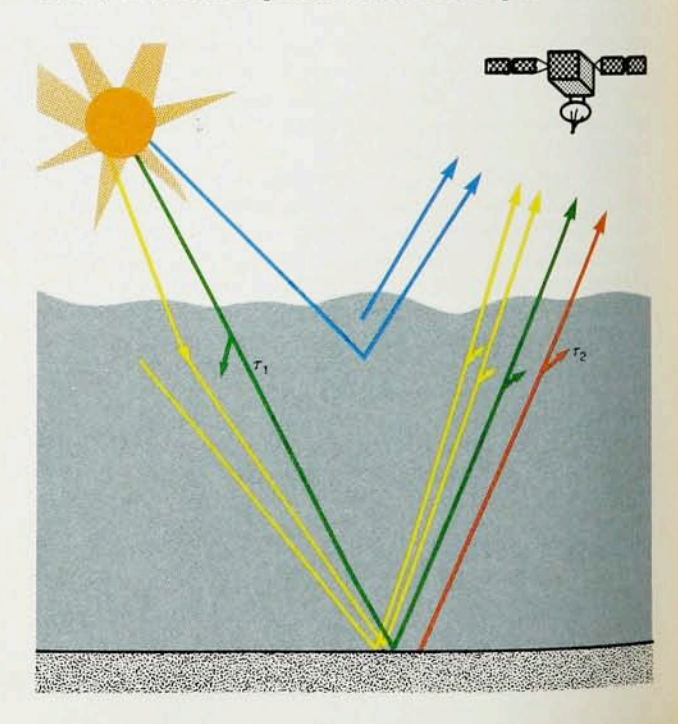
$$L = (1/\pi)E\tau_1 r \tau_2 + L_{\rm d} r \tau_2 + \epsilon L_{\rm b} \tau_2 + L_{\rm u}$$
 (1)

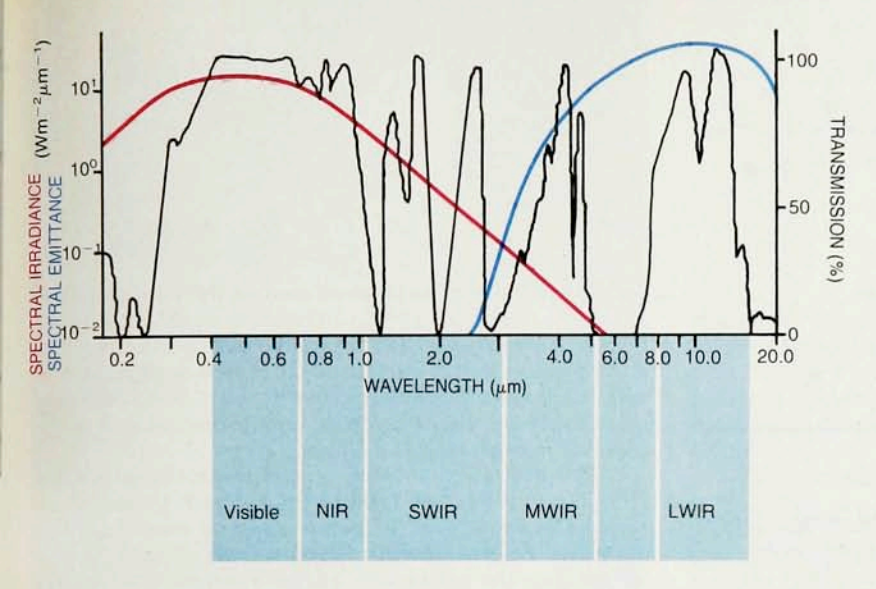
where L is the spectral radiance seen by a detector above the atmosphere; E is the spectral irradiance of the sunlight as it strikes the top of the atmosphere;  $\tau_1$  and  $\tau_2$  are the transmission coefficients of the atmosphere along the Sun–Earth and Earth–sensor paths, respectively; r is the reflectance of the ground cover;  $L_{\rm d}$  is the "down-

The four main energy paths that enter into remote-sensing calculations are: sunlight that is transmitted through the atmosphere, reflected off the Earth and transmitted back up through the atmosphere (shown in green above); radiation that is either emitted or scattered downward by the atmosphere, reflects off some ground cover and passes back up through the atmosphere to the detector (yellow); blackbody radiation emitted by the ground cover (orange); and radiation either scattered upward or emitted by the atmosphere (blue). Each energy path contributes one term to equation 1 (see text). The shortest arrows indicate attenuation due to atmospheric absorption and scattering. Figure 3

welled" spectral radiance, a combination of the sunlight scattered downward by the atmosphere and the downward thermal emission from the atmosphere;  $L_{\rm u}$  is the "upwelled" spectral radiance, a combination of the sunlight scattered upward by the atmosphere and the upward thermal emission from the atmosphere;  $L_{\rm b}$  is the spectral radiance from an ideal blackbody at the same temperature as the ground cover; and  $\epsilon$  is the emissivity of the ground cover.  $L, L_{\rm d}, L_{\rm u}$  and  $L_{\rm b}$  are expressed in Wm $^{-2}\mu$ m $^{-1}$ sr $^{-1}$ ; E is in Wm $^{-2}\mu$ m $^{-1}$ ;  $\tau_1$ ,  $\tau_2$ ,  $\tau_1$  and  $\epsilon$  are all wavelength dependent.

Depending on the spectral sensitivity of the sensor, the signal it records carries information about the reflectance and thermal properties of the Earth, or some combination thereof. This is illustrated in figure 4, which shows the irradiance from the Sun outside the atmosphere, the radiant emittance from a blackbody at 300 K and the transmission spectrum of the Earth's atmosphere. Earth remote sensing is restricted to "windows" (passbands) in the atmospheric transmission spectrum. As is





Spectra that are important for remote sensing. The solar spectrum (red curve; left axis) and the blackbody spectra of ground sources, typified by the 300-K blackbody spectrum shown above (blue curve; left axis), represent the two main radiation sources used in remote sensing. The transmission spectrum of the Earth's atmosphere (black curve; right axis) has two "windows" that permit observation near the high-power points of the two source spectra: One window is in the visible-near-infrared, the other, in the long-wave infrared. (In this figure, it is assumed that the solar spectrum is measured just outside the Earth's atmosphere, whereas the blackbody radiation from ground sources is measured at ground level.) Figure 4

evident from figure 4, the two dominant windows for remote sensing are in the visible—near-infrared and in the long-wave infrared. In the signal reaching an airborne or satellite detector, the energy in the visible and near-infrared is sunlight reflected from the Earth, which contains information about the texture and chemical composition of the ground cover. In the long-wave infrared, nearly all the energy is blackbody emission from the Earth, which carries detailed information about the surface temperature. Thus, in the visible—near-infrared, equation 1 reduces to

$$L = (1/\pi)E\tau_1 r \tau_2 + L_{\rm d} r \tau_2 + L_{\rm u}$$
 (2)

and in the long wave infrared, to

$$L = \epsilon L_{\rm b} \tau_2 + L_{\rm d} r \tau_2 + L_{\rm u} \tag{3}$$

It is important to recognize that the  $L_d$  and  $L_u$  terms are due to scattered solar photons in equation 2 and to blackbody photons emitted by the atmosphere in equation 3. These simplifications are not valid in the midwave infrared region or for very hot objects. In the midwave infrared, images are often difficult to interpret because they are due to a mixture of reflected and thermally emitted photons. Inspection of equations 2 and 3 reveals that under clear conditions with a homogeneous atmosphere, the primary spatial variables are the reflectance in equation 2, and the emittance due to the temperature and emissivity of the ground cover in equation 3. Thus variations in brightness can be directly correlated with variations in the quantities of interest. Methods for rigorously solving equations 2 and 3 are the subject of much ongoing research, some of which is reviewed in reference 4.

### Film-camera sensors

A comprehensive treatment of the sensors used for Earth observation is beyond the scope of this article, but it is worthwhile reviewing some selected sensors used for applications of general interest to the physics community. (More comprehensive discussions can be found in the literature cited throughout the article.)

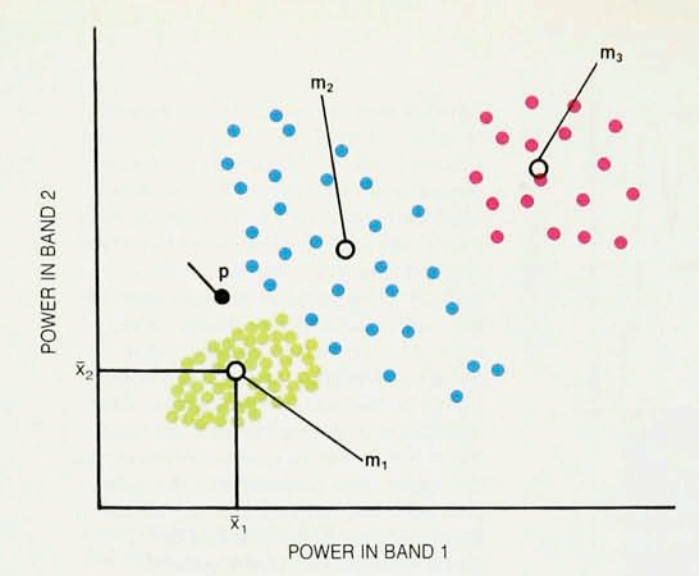
The low cost and high resolution of photographic film make it the most widely used imaging sensor for manned space missions. The Gemini, Apollo and Skylab missions acquired large volumes of imagery using a variety of filmcamera combinations. In many cases the cameras were

commercial 35-mm or 70-mm models, often with larger film magazines and lenses of longer focal length added to accommodate mission requirements. Special cameras with larger fields of view and higher resolution were also developed for the manned missions. The large-format camera developed for use on the space shuttle is a good example: The film format is  $230\!\times\!460$  mm, with ground resolutions of the order of 15 m per resolvable line pair. The image area covers  $225\!\times\!450$  km from a typical shuttle altitude of 300 km. Through the use of various film–filter combinations, cameras can acquire images over the visible and near-infrared portion of the spectrum.

### Multispectral electro-optical sensors

Despite its low cost and high resolution, photographic film has some severe drawbacks for space-based imaging. Chief among these are the finite film payload (which limits system data capacity) and the necessity of returning exposed film to Earth for interpretation and analysis. For long-term Earth resource assessment-often done at high altitudes, where returning the film becomes particularly difficult-electro-optical sensors are preferable. The scanners flown on Landsats 4 and 5 are such sensors. They are commonly called "whisk broom" scanners, because they collect data by oscillating a mirror back and forth as they move over the land, and in this fashion observe a swath of land directly underneath them. Using an array of spectrally filtered detectors, arranged so that each parcel of land corresponding to a pixel is sampled in each of the detectors, these scanners generate multispectral images. The Multispectral Scanner uses silicon photodiode detectors in the longest infrared band and photomultiplier detectors at all shorter wavelengths. It has four spectral channels and a 76-m ground instantaneous field of view (see table 1). The Thematic Mapper employs solid-state detectors for six reflective bands (30-m gifov) and one thermal band (120-m gifov).

The MSS and TM sensors have been used for extensive Earth resource studies, in which detailed maps of ground features are derived from spectral information using the techniques of statistical pattern recognition. Figure 5 provides an example of how such techniques are used. The digital representation of the brightness of a pixel in each of the *n* spectral bands defines a point in an *n*-dimensional space. Pixels that belong to a single class of land cover type tend to cluster together in this space because of their



Pixels in a hypothetical Earth image. Each pixel may be represented as a point in n dimensions ("spectral vector"), whose components are simply the power detected in each of the n wavelength bands. The different land cover types form clusters in this n-dimensional space, which can be identified using pattern recognition algorithms. This figure illustrates the simple case of n = 2. The simplest pattern recognition algorithms classify data points by their distances from the mean points in each cluster. To initially calculate these mean points, one uses small "training data" sets. The mean points for the three hypothetical ground cover types in this figure are labelled  $m_1$ ,  $m_2$  and  $m_3$ ;  $\bar{x}_1$  and  $\bar{x}_2$  are the components of m<sub>1</sub>—the mean values in each spectral band. The black point, p, represents a pixel of unknown land cover type. Figure 5

similar radiometric signatures. Such clustering can be quantified via a variety of statistical techniques<sup>5</sup> and used to identify the land cover classes. At present, spectral pattern recognition still relies heavily on a human analyst in the initial interpretation, or "training," phase of the algorithms, in which a small number of pixels in each cluster must be identified as representing a particular type of land cover. This need for human analysis arises largely because the data depend on illumination and atmospheric effects (as described by equation 1), which vary with each new image. Much ongoing research is aimed at developing techniques to remove or minimize atmospheric effects. However, even with these effects present, numerous investigations have demonstrated the usefulness of Landsat spectral data for studying a variety of water, crop, forest, soil and geological resource issues when assisted by human analysts or when the image data are correlated with ground "truth" measurements. In particular, the synoptic perspective that such data provide—50 000 km<sup>2</sup> may be covered by a single image—is invaluable for studies of large-scale phenomena or for extrapolating detailed knowledge of a small region to a much larger area.

In addition to the Landsat satellites, a number of National Oceanic and Atmospheric Administration satellites are equipped with electro-optical sensors. The Advanced Very High Resolution Radiometer has an optical system similar to those used on the Landsats. The AVHRR has multiple spectral channels in the visible and infrared (see table 1). It is characterized by relatively low spatial resolution (1-km gifov at nadir), a wide field of view and essentially daily coverage. It has been used extensively for global resource monitoring, as well as for detailed meteorological studies.

The newest generation of satellite scanners employ charge-coupled-device technology in "push broom" scanners. The French SPOT sensor is a good example of this approach. Linear arrays of thousands of detector elements span the entire focal plane. Each array samples a line of data, and the forward motion of the spacecraft allows line after line to be sampled. Through the placement of different filters over several parallel arrays, multispectral data are acquired. SPOT uses a pointing mirror to acquire imagery at off-nadir angles of up to + 27°, which facilitates repeat coverage on orbits in which the study site is not directly overflown. The directability of the mirror also enables SPOT to acquire stereo imagery for topographic mapping. The high resolution (10-m GIFOV panchromatic, 20-m gifov multispectral) of the SPOT sensor is illustrated by the image shown in figure 6.

## Hyperspectral sensors

Probably the most exciting recent development in imaging sensors is the hyperspectral sensor. Multispectral sensors such as SPOT, TM, AVHRR and MSS all sample the electromagnetic spectrum over bands approximately 100 nm wide. Sensors with this kind of spectral resolution allow us to isolate only broad spectral features, severely limiting the degree of possible material or land cover classification. Hyperspectral instruments, on the other hand, sample the spectrum over bands roughly one-tenth as wide. (Hyperspectral systems may sample 100 or more reflective bands, whereas TM samples only six.) Therefore one can potentially extract much more detailed information about material types from the hyperspectral data.

NASA has tried two approaches for acquiring such data, embodied in two experimental sensors: the airborne image spectrometer, AIS-2, and the Advanced Visible-Infrared Imaging Spectrometer. These airborne sensors are being used to assist in understanding the characteristics of the proposed space-based imaging spectrometers, HIRIS and MODIS (see table 2), which are to be launched in the mid-1990s. Figure 7 is an example of an AVIRIS image. It was generated as a three-band color composite with the color-coded spectral data for the edge pixels shown in the third dimension to provide insight into how the 220 separate spectral images might appear.

The low resolution (1 milliradian, as opposed to roughly 12 microradians for SPOT) of this airborne system is an indication of the trade-off between spatial and spectral resolution inherent in remote imaging. The limited number of photons reaching the sensor from an object can be divided into so many spectral bands or so many pixels per object, but not both. Improved signal-to-noise and higher spatial resolution require larger collections.



Table 1. Spaceborne imaging systems 8.9

System (sensor type)	Spectral bands (μm)	Resolution	Orbit type Polar	
Landsat TM (Whisk broom)	0.45-0.52 0.52-0.60 0.63-0.69 0.76-0.90 1.55-1.75 2.08-2.35 10.4-12.5	30-m GIFOV in 1st 6 bands; 120-m GIFOV in 7th		
Landsat MSS (Whisk broom)	0.5-0.6 0.6-0.7 0.7-0.8 0.8-1.1 10.4-12.6	76-m GIFOV in 1st 4 bands; 234-m GIFOV in 5th	Polar	
SPOT (Push broom)	0.50-0.59 0.61-0.69 0.79-0.90 0.50-0.90	20-m GIFOV multispectral (first 3 bands); 10-m GIFOV panchromatic (4th band)	Polar	
Vissr (Line scanner)	0.55-0.75 (visible); 10.5-12.6 (ir)	0.9-km GIFOV (visible); 8-km GIFOV (ir)	Geosta- tionary	
HCMM (Line scanner)	0.55–1.1 (visible); 10.5–12.5 (ir)	0.5-km GIFOV (visible); 0.6-km GIFOV (ir)	Polar	
AVHRR (Line scanner)	0.58-0.68 0.725-1.10 3.55-3.93 10.5-11.5 11.5-12.5	1-km GIFOV (local coverage); 4-km GIFOV (global coverage)	Polar	
arge format Film-depend- camera ent		Film-dependent (15 m/resolv- able line pair or better at 300-km altitude)	Usually near- equatorial	

The great pyramids. This panchromatic view, taken by SPOT, has a GIFOV of 10 m. The figure is a small section of an image that has been spatially and radiometrically enhanced to accentuate resolution and reduce noise. The angular resolution in this image is close to the limits of civilian sensors. Figure 6

tion optics or longer dwell times (that is, slower scanning). Since large optics are expensive, particularly in space, and scan rates are largely dictated by orbital dynamics (or, in airborne systems, airplane speed), the struggle beween spatial and spectral resolution will continue into the near future.

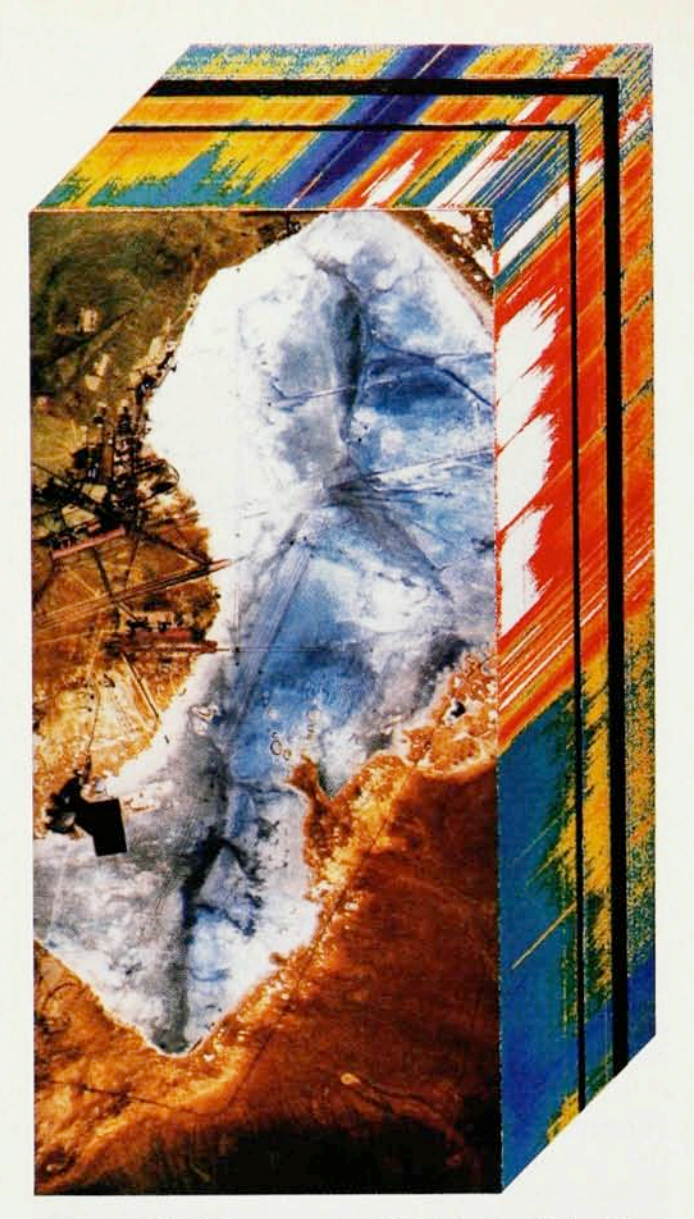
An important feature to note in the spectra of figure 7 is that they are strongly influenced by the transmission spectrum of the atmosphere. This problem, common to all spectral data, makes it more difficult to match airborne or satellite spectra with libraries of laboratory or field spectra.

Many current techniques use atmospheric propagation models in an attempt to characterize and remove atmospheric effects. And ongoing research is aimed at utilizing the spectral information in the image itself to remove atmospheric effects from the spectra of the surface objects. In either case, high-speed, accurate methods using algorithms that compare and match spectra to classify and analyze surface conditions (such as crop health) must be developed. Because the quantities of data are huge (a hiris scene representing  $30\times30$  km on the ground will contain approximately 300 megabytes of data), conventional data analysis techniques on existing computers are cumbersome. The more detailed questions that can be addressed by hyperspectral data will call for new image analysis techniques and computer technology.

### Thermal infrared sensors

One can consider thermal infrared sensors as simply another type of detector at the focal plane of a multispectral imaging system. For example, Landsat and AVHRR have thermal sensors as well as visible and short-wave infrared sensors. Nonetheless, the technologies and requirements of thermal sensors are qualitatively different in several ways. For example, because the energies of the signal are much lower relative to ambient sources the detectors must be cooled to cryogenic temperatures to reduce background noise. In addition, every optical element has a temperature above absolute zero and is therefore self-radiating. This background radiance level makes special monitoring and calibration techniques necessary when making precise measurements. The most fundamental difference, of course, is in the information contained in the image itself. In the long-wave infrared region, where most thermal sensing occurs, the detected signal is predominantly a function of the temperature and emissivity of the imaged objects as modified by the atmospheric transmission and path radiance effects described in equation 3. Thus for objects with roughly constant emissivity values, in homogeneous atmospheric conditions, brightness is a function only of temperature.

For example, the bright band around Lake Ontario in the left panel of figure 8 represents a ring of much warmer water in the near-shore area, evidence of the thermal bar phenomenon, which occurs each spring in large, temperate-zone lakes. For several weeks in the springtime, the shore waters exhibit summer stratification (warm water



on top), while the core water of the lake is still in winter stratification (cold water on top). The interface between these regions occurs at a bar of sinking water at 4 °C, the temperature of maximum water density. The thermal bar slowly migrates outward from the shore, and eventually Hyperspectral image of Rogers Dry Lake in California, taken by AVIRIS. The lake bed is shown in a false-color composite. in which red represents a wavelength of 0.690 µm; green, 1.534 µm; and blue, 2.222 µm. The runways at Edwards Air Force Base are clearly visible at the left, extending onto the lake bed. The multicolored strip seen in perspective shows the complete spectra of the pixels along two edges of the rectangular image. Moving "into the page," the wavelengths are increasing, from 0.4  $\mu m$  to 2.45  $\mu m$ . The black bands in the spectra of the edge pixels show the atmospheric H2O absorption at 1.4 and 1.9 µm. (Courtesy of Gregg Vane, NASA and the Jet Propulsion Laboratory.) Figure 7

disappears when the lake fully stratifies in summer.

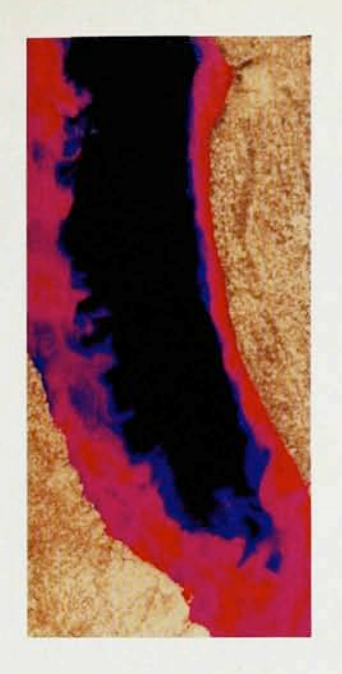
The right panel of figure 8 illustrates the value of having visible-near-infrared data in conjunction with thermal data. After digital processing to accentuate the reflectance variations, visible-band data from Landsat clearly show the turbidity variations induced by the thermal bar. Runoff from snow melt and spring storms carries sediments and pollutants into the lake, which are trapped in the warm near-shore waters by the thermal barrier. The resultant high concentrations of suspended solids and chlorophyll in the near-shore waters cause the observed turbidity pattern. The near-shore turbidity is of only mild concern in itself, but it is strongly correlated with less visible, but more harmful, pollutants trapped near the shore by the thermal bar. Satellite images reveal the interplay between temperature and turbidity that occurs in the thermal bar phenomenon with a synoptic perspective unachievable by any other means.7

Thermal images have also been used extensively to monitor cloud patterns and movement. The Geostationary Operational Environmental Satellites use a visible channel during the day and a long-wave infrared channel day and night, generating images of a full hemisphere every half-hour. Each of the cylindrical GOES satellites

Table 2. Hyperspectral imaging systems

System	Sensor type	Spectral range (μm)	Spectral bandwidth (nm) (approx.)	Resolution	No. of pixels per line	No. of spectral bands
AIS-2	2-D array	0.8–1.6 or 1.2–2.4	10	2.05 milliradians/ pixel	64	128
Aviris	Linear array	0.4-2.45	10	1 milliradian/ pixel	550	224
Hiris	Push broom area array	0.4–2.5	10	30-m gifov	1000	192
Modis N	Whisk broom scanner array	0.4–12	Varies (1.2–500)	500-m or 1000-m gifov (depending on wavelength)	1500 or 3000 (depending on wavelength)	36

Lake Ontario in the springtime, as seen by the TM scanner aboard Landsat. These images illustrate the thermal bar phenomenon. The false-color image of the thermal band (10.4–12.5 μm) at left shows warmer temperatures on the surface of the in-shore waters. Black represents cold temperatures (< 4 °C), and the temperature increases from blue through red. The enhanced true-color image at right shows the turbidity variations accompanying the thermal phenomenon (see figure 2). In this image, red represents the 0.63–0.69 μm band; green, the 0.52–0.60 μm band; and blue, the 0.45–0.52 μm band. Figure 8





rotates about its central axis, generating a scan of the direction parallel to the equator, while a mirror slowly oscillates from pole to pole. The low-resolution images the GOES satellites produce often appear in television weather reports.

The AVHRR, particularly its thermal channels, can be used to assess cloud patterns in greater detail than the GOES sensor provides, though with less frequent coverage (twice daily). The long-wave infrared images are used to study and monitor the locations of clouds and to estimate their altitudes. This is possible because cloud brightness is proportional to temperature to a good approximation, and at higher altitudes the temperature is quite predictable.

By appropriate selection of orbits, it is possible to orient a satellite such that it will periodically pass over a target near the thermal extrema of the diurnal cycle. The Heat Capacity Mapping Mission studied a variety of phenomena that exhibit different levels of thermal inertia using just this technique. For example, moist soils change temperature to a lesser degree than dry soils over the daily solar heating cycle. Figure 1 is an HCMM image of the East Coast, taken during the hottest portion of the day. Localized heating is apparent in several major urban regions. This phenomenon—the "urban heat island"—is due to a combination of factors, including low thermal inertia due to material properties, low daytime cooling due to a lack of evaporation through foliage (evapotranspiration) and low wind conditions (created in part by buildings, and perpetuated by the higher temperatures). In summer, the same conditions that cause heat island formation can also trap air pollutants in the urban core and result in a significant health threat. Once again, satellite data are matchless for monitoring the magnitude and extent of the phenomenon; the data also aid in studies of how it is ameliorated by neighborhood parks and green spaces.

# Imaging comes of age

In 30 years, spaceborne imaging has grown from a few experimental photographs to a continuous stream of images from a host of operational and research instruments. The suite of sensors and analysis techniques has expanded to permit studies of every major aspect of Earth resources, including meteorology, oceanography, water resources, geology, geography, cartography, soil science, agriculture, forestry and land management. The ques-

tions being asked are changing from "Is it observable?" to "How well can it be measured?" The concern is no longer simply whether or not an area is agricultural, but what is growing there, what the soil moisture is, and what the condition of the crop is in terms of health and potential yield.

The tools to address these questions are not yet all at hand, but ongoing improvements in computer technology and new algorithms and techniques for image processing and analysis suggest that such tools will be available soon. New or improved atmospheric models will enable us to better understand and account for atmospheric effects and energy-matter interactions. The infant science of data fusion should provide major advances by providing the ability to merge images from many different sensors with a range of spatial and spectral resolutions and acquisition times. And it will be possible to merge image data with data from other sensors, with data bases, with improved physical models of the imaging and radiometric processes, and with models of the phenomena under study. If spaceborne imaging has matured from infancy to adolescence in the past three decades, over the next several decades the science will come of age in its role of providing local- and global-scale information about the state of the planet.

### References

- D. S. Simonette, ed. of chap. 1, Manual of Remote Sensing, 2nd ed., vol. 1, Am. Soc. of Photogrammetry, Falls Church, Va. (1983).
- T. M. Lillesand, R. W. Kiefer, Remote Sensing and Image Interpretation, 2nd ed., Wiley, New York (1987).
- R. N. Colwell, ed., Manual of Remote Sensing, 2nd ed., vols. 1 and 2, Am. Soc. of Photogrammetry, Falls Church, Va. (1983).
- P. N. Slater, Remote Sensing: Optics and Optical Systems, Addison-Wesley, Reading, Mass. (1980).
- R.O. Duda, P.E. Hart, Pattern Classification and Scene Analysis, Wiley, New York (1973).
- A. F. H. Goetz, G. Vane, J. Solomon, B. N. Rock, Science 228, 1147 (1985).
- 7. J. R. Schott, Remote Sensing Rev. 1, 1 (1985).
- H. S. Chen, Space Remote Sensing Systems, Academic, New York (1985)
- Proc. of the Landsat-4 Early Results Symp., NASA Conf. Publ. 2326, Vol. 1, NASA, Washington DC (1983).